

Far-UVC light efficiently and safely inactivates airborne human coronaviruses

CURRENT STATUS: UNDER REVIEW

nature research

Manuela Buonanno

Center for Radiological Research, Columbia University Irving Medical Center, New York, New York 10032, USA

David Welch

Center for Radiological Research, Columbia University Irving Medical Center, New York, New York 10032, USA

Igor Shuryak

Center for Radiological Research, Columbia University Irving Medical Center, New York, New York 10032, USA

David J. Brenner

Center for Radiological Research, Columbia University Irving Medical Center, New York, New York 10032, USA

DOI:

10.21203/rs.3.rs-25728/v1

SUBJECT AREAS

Virology

KEYWORDS

aerosolized coronavirus, beta HCoV-OC43, alpha HCoV-229E, far-UVC light,

Abstract

A direct approach to limit airborne transmission of pathogens is to inactivate them within a short time of their production. Germicidal ultraviolet light (UV), typically at 254 nm, is effective in this context, but it is a health hazard to the skin and eyes. By contrast, far-UVC light (207-222 nm) efficiently kills pathogens without harm to exposed human cells or tissues. We previously demonstrated that 222-nm UV light efficiently kills airborne influenza virus (H1N1); here we extend the far-UVC studies to explore efficacy against human coronaviruses from subgroups alpha (HCoV-229E) and beta (HCoV-OC43). We found that low doses of, respectively 1.7 and 1.2 mJ/cm² inactivated 99.9% of aerosolized alpha coronavirus 229E and beta coronavirus OC43. Based on these results for the beta HCoV-OC43 coronavirus, continuous far-UVC exposure in public locations at the currently recommended exposure limit (3 mJ/cm²/hour) would result in 99.9% viral inactivation in ~ 25 minutes. Increasing the far- UVC intensity by, say, a factor of 2 would halve these disinfection times, while still maintaining safety. As all human coronaviruses have similar genomic size, a key determinant of radiation sensitivity, it is realistic to expect that far-UVC light will show comparable inactivation efficiency against other human coronaviruses, including SARS-CoV-2.

Introduction

Coronavirus disease 2019 (COVID-19) was first reported in December 2019 and then characterized as a pandemic by the World Health Organization on March 11, 2020. Despite extensive efforts to contain the spread of the disease, it has spread worldwide with over 1.9 million confirmed cases and over 130,000 confirmed deaths as of April 16, 2020 ¹. Transmission of SARS-CoV-2, the beta coronavirus causing COVID-19, is both through direct contact and airborne routes, and studies of SARS-CoV-2 stability have shown viability in aerosols for at least 3 hours ². Given the rapid spread of the disease, including through asymptomatic carriers ³, it is of clear importance to explore practical mitigation technologies that can inactivate the airborne virus in public locations and thus limit airborne transmission.

Ultraviolet (UV) light exposure is a direct antimicrobial approach ⁴ and its effectiveness against

different strains of airborne viruses has long been established ⁵. The most commonly employed type of UV light for germicidal applications is a low pressure mercury-vapor arc lamp, emitting around 254 nm; more recently xenon lamp technology has been used, which emits broad UV spectrum ⁶. However, while these lamps can be used to disinfect unoccupied spaces, operation of these conventional germicidal UV lamps in occupied public spaces - critical to prevent person-to-person transmission - is not possible since exposure to these wavelengths is a health hazard, causing both skin cancer and eye diseases ⁷⁻¹⁰.

By contrast far-UVC light (207 to 222 nm) has been shown to be as efficient as conventional germicidal UV light in killing microorganisms ¹¹, but it does not have the human health issues associated with conventional germicidal UV light. In short (see below) the reason is that far-UVC has a range in biological materials of only a few micrometers, and thus it cannot reach living human cells in the skin or eyes. But because viruses (and bacteria) are extremely small, far-UVC light can still penetrate and kill them. Thus far-UVC light has about the same highly effective germicidal properties of UV light, but without the associated human health risks ¹²⁻¹⁵. Several groups have thus proposed that far-UVC light (207 or 222 nm), which can be generated using inexpensive excimer lamps, is a potential safe and efficient anti-microbial technology ¹²⁻¹⁸ which can be deployed in occupied public locations.

The physics-based mechanistic basis to this far-UVC approach ¹² is that light in this wavelength range has a very limited penetration depth. Specifically, far-UVC light (207-222 nm) is very strongly absorbed by proteins through the peptide bond, and other biomolecules ^{19,20}, so its ability to penetrate biological materials is very limited compared with, for example, 254 nm (or higher) conventional germicidal UV light ^{21,22}. This limited penetration is still much larger than the size of viruses and bacteria, so far-UVC light is as efficient in killing these pathogens as conventional germicidal UV light ¹²⁻¹⁴. However, unlike germicidal UV light, far-UVC light cannot penetrate either the human stratum corneum (the outer dead-cell skin layer), nor the ocular tear layer, nor even the

cytoplasm of individual human cells. Thus, far-UVC light cannot reach or damage living cells in the human skin or the human eye, in contrast to the conventional germicidal UV light which can reach these sensitive cells ⁷⁻¹⁰.

In summary far-UVC light is anticipated to have about the same anti-microbial properties as conventional germicidal UV light, but without producing the corresponding health effects. Should this be the case, far-UVC light has the potential to be used in occupied public settings to prevent the airborne person-to-person transmission of pathogens such as coronaviruses.

We have previously shown that a very small dose (2 mJ/cm^2) of far-UVC light at 222 nm was highly efficient in inactivating aerosolized H1N1 influenza virus ²³. In this work we explore the efficacy of 222 nm light against two airborne human coronaviruses: alpha HCoV-229E and beta HCoV-OC43. Both were isolated over 50 years ago and are endemic to the human population, causing 15–30% of respiratory tract infections each year ²⁴. Like SARS-CoV-2, the HCoV-OC43 virus is from the beta subgroup ²⁵.

Here we measured the efficiency with which far-UVC light inactivates these two human coronaviruses when exposed in aerosol droplets of sizes similar to those generated during sneezing and coughing ²⁶. As all coronaviruses have comparable physical and genomic size, a critical determinant of radiation response ²⁷, we hypothesized that both viruses would respond similarly to far-UVC light, and indeed that all coronaviruses will respond similarly.

Results

Inactivation of human coronaviruses after exposure to 222 nm light in aerosols
Infectivity Assay. We used a standard approach to measure viral inactivation, assaying coronavirus infectivity in human host cells (normal lung cells), in this case after exposure in aerosols to different doses of far-UVC light. We quantified virus infectivity with the 50% tissue culture infectious dose TCID₅₀ assay ²⁸, and estimated the corresponding plaque forming units (PFU)/ml using the conversion $\text{PFU/ml} = 0.7 \text{ TCID}_{50}$ ²⁹. Fig. 1 shows the fractional survival of aerosolized coronaviruses HCoV-229E and HCoV-OC43 expressed as $\text{PFU}_{\text{UV}}/\text{PFU}_{\text{controls}}$ as a function of the incident 222-nm dose. Robust

linear regression (Table 1) using iterated reweighted least squares³⁰ indicated that the survival of both subgroups alpha and beta is consistent with a classical exponential UV disinfection model ($R^2 = 0.86$ for HCoV-229E and $R^2 = 0.78$ for HCoV-OC43). For the alpha coronavirus HCoV-229E, the inactivation rate constant (susceptibility rate) was $k = 4.1 \text{ cm}^2/\text{mJ}$ (95% confidence intervals (C. I.) 2.5–4.8) which corresponds to an inactivation cross-section (or the dose required to kill 90% of the exposed viruses) of $D_{90} = 0.56 \text{ mJ}/\text{cm}^2$. Similarly, the susceptibility rate for the beta coronavirus HCoV-OC43 was $k = 5.9 \text{ cm}^2/\text{mJ}$ (95% C. I. 3.8–7.1) which corresponds to an inactivation cross section of $D_{90} = 0.39 \text{ mJ}/\text{cm}^2$.

Viral Integration Assay. We investigated integration of the coronavirus in human lung host cells, again after exposure in aerosols to different doses of far-UVC light. Figs. 2 and 3 show representative fluorescent 10x images of human lung cells MRC-5 and WI-38 incubated, respectively, with HCoV-229E (Fig. 2) and HCoV-OC43 (Fig. 3), which had been exposed in aerosolized form to different far-UVC doses. The viral solution was collected from the BioSampler after running through the aerosol chamber while being exposed to 0, 0.5, 1 or 2 mJ/cm^2 of 222-nm light. Cells were incubated with the exposed virus for one hour, the medium was replaced with fresh infection medium, and immunofluorescence was performed 24 hours later. We assessed the human cell lines for expression of the viral spike glycoprotein, whose functional subunit S2 is highly conserved among coronaviruses^{31,32}. In Figs. 2 and 3, green fluorescence (Alexa Fluor®-488 used as secondary antibody against anti-human coronavirus spike glycoprotein antibody) qualitatively indicates infection of cells with live virus, while the nuclei were counterstained with DAPI appearing as blue fluorescence. For both alpha HCoV-229E and beta HCoV-OC43, exposure to 222-nm light reduced the expression of the viral spike glycoprotein as indicated by a reduction in green fluorescence.

Discussion

The severity of the 2020 COVID-19 pandemic warrants the rapid development and deployment of effective countermeasures to reduce person-to-person transmission. We have developed a promising

approach using single-wavelength far-UVC light at 222 nm generated by filtered excimer lamps, which inactivate viruses and bacteria, without inducing biological damage in exposed human cells and tissue 11-16. The approach is based on the biophysically-based principle that far-UVC light, because of its very limited penetration in biological materials, can traverse and kill viruses and bacteria which are typically micrometer dimensions or smaller, but it cannot penetrate even the outer dead-cell layers of human skin, nor the outer tear layer on the surface of the human eye ¹².

In this work we have used an aerosol irradiation chamber to test the efficacy of 222-nm far-UVC light to inactivate two aerosolized human coronaviruses, beta HCoV-OC43 and alpha HCoV-229E. As shown in Fig. 1, inactivation of the two human coronavirus by 222-nm light follows a typical exponential disinfection model, with an inactivation constant for HCoV-229E of $k = 4.1 \text{ cm}^2/\text{mJ}$ (95% C. I. 2.5-4.8), and $k = 5.9 \text{ cm}^2/\text{mJ}$ (95% C. I. 3.8-7.1) for HCoV-OC43. These values imply that 222 nm UV light doses of only $1.7 \text{ mJ}/\text{cm}^2$ or $1.2 \text{ mJ}/\text{cm}^2$ respectively produce 99.9% (3-log reduction) of aerosolized alpha HCoV-229E or beta HCoV-OC43. A summary of k values and the corresponding D_{90} , D_{99} , and $D_{99.9}$ values we have obtained for coronaviruses is shown in Table 2, together with our earlier results for aerosolized H1N1 influenza virus ²³.

The results suggest that both of the studied coronavirus strains have similar high sensitivity to far-UVC inactivation. Robust linear regression produced overlapping 95% confidence intervals for the inactivation rate constant, k , of 2.5 to 4.8 cm^2/mJ and 3.8 to 7.1 cm^2/mJ respectively for the 229E and OC43 strains. As all human coronaviruses have similar genomic sizes which is a primary determinant of UV sensitivity ²⁷, it is reasonable to expect that far-UVC light will show similar inactivation efficiency against all human coronaviruses, including SARS-CoV-2. The data obtained here are consistent with this hypothesis.

It is useful to compare the performance of far-UVC light with conventional germicidal (peak 254 nm) UVC exposure. We are aware of only one such study ³³, which used an aerosolized murine beta coronavirus. The study reported a D_{88} of $0.599 \text{ mJ}/\text{cm}^2$, which others ⁴ have used to estimate the D_{90}

for the virus with 254 nm light as 0.6 mJ/cm². This value is similar to those estimated in the current work (see Table 2), suggesting similar inactivation efficiency of 222 nm far-UVC and conventional germicidal 254 nm UVC for aerosolized coronavirus, and providing further support for the suggestion that all coronaviruses have similar sensitivities to UV light.

The sensitivity of the coronaviruses to far-UVC light, together with extensive safety data even at much higher far-UVC exposures ¹²⁻¹⁸, suggests that it will be feasible and safe to have the lamps providing continuous far-UVC exposure in public places to significantly reduce the probability of person-to-person transmission of coronavirus as well as other seasonal viruses such as influenza. For example, the current dose limit guideline for 222 nm light from the International Commission on Non-ionizing Radiation Protection (ICNIRP) is 23 mJ/cm² per 8-hour exposure ³⁴. Interpreting this as an intensity of ~3 mJ/cm²/hour, and based on our results here for the beta HCoV-OC43 coronavirus, continuous far-UVC exposure at this intensity would result in 90% viral inactivation in approximately 8 minutes, 95% viral inactivation in approximately 11 minutes, 99% inactivation in approximately 16 minutes and 99.9% inactivation in approximately 25 minutes. Increasing the intensity by, say, a factor of 2 would halve these disinfection times, while still maintaining safety ¹²⁻¹⁸.

In conclusion, we have shown that very low doses of far-UVC light efficiently kill airborne human coronaviruses carried by aerosols. An exposure dose as low as 1.2 to 1.7 mJ/cm² of 222-nm light inactivates 99.9% of the airborne human coronavirus tested from both subgroups beta and alpha, respectively. Together with previous safety studies ¹²⁻¹⁸ and our earlier studies with aerosolized influenza A (H1N1) ²³, these results indicate that far-UVC light is a potentially powerful and practical approach for reduction of airborne viral transmission, without the human health hazards associated with conventional germicidal UVC lamps.

These results suggest the utility of deploying low dose rate far-UVC lights in highly occupied indoor public locations such as hospitals, transportation vehicles, airports and schools, potentially representing a safe and inexpensive tool to reduce the spread of airborne-mediated microbial

diseases.

Far-UVC technology can potentially help limit seasonal influenza epidemics, transmission of measles and tuberculosis, as well as future pandemics.

Methods

Viral Strains. HCoV-229E (VR-740) and HCoV-OC43 (VR-1558) were propagated in human diploid lung MRC-5 fibroblasts (CCL-171) and WI-38 (CCL-75), respectively (all from ATCC, Manassas, VA). Both human cell lines were grown in MEM supplemented with 10% Fetal Bovine Serum (FBS), 2 mM L-alanyl-L-glutamine, 100 U/ml penicillin and 100 µg/ml streptomycin (Sigma-Aldrich Corp. St. Louis, MO, USA). The virus infection medium consisted of MEM or RPMI-1640 plus 2% heat inactivated FBS for HCoV-229E and HCoV-OC43, respectively. The viral strains were propagated by inoculation of flasks containing 24-hours old host cells, which were 80-90% confluent. After one hour incubation, the cell monolayer was washed and incubated in fresh infection medium for three or four days at 35°C for HCoV-229E and at 33°C for HCoV-OC43. The supernatant containing the working viral stock was then collected by centrifugation (300 g for 15 minutes). The virus titer was determined by 50% tissue culture infective dose TCID₅₀ by assessing cytopathic effects (CPE), which were scored at a bright field microscope (10x) as vacuolization of cytoplasm, cell rounding and sloughing.

Benchtop Aerosol Irradiation Chamber. A one-pass, dynamic aerosol/virus irradiation chamber was used to generate, expose, and collect aerosol samples as previously described²³. Viral aerosols were generated by adding a virus solution in a high-output extended aerosol respiratory therapy nebulizer (Westmed, Tucson, AZ) and operating using an air pump with an input flow rate of 11 L/min. Virus flowed into the chamber and was mixed with dry and humidified air to maintain humidity between approximately 50-70%. The relative humidity, temperature, and aerosol particle size distribution were monitored throughout operation. Aerosol was exposed to far-UVC light and finally collected using a Biosampler (SKC Inc., Eighty Four, PA).

The far-UVC lamp was positioned approximately 22 cm away from the UV exposure chamber and directed at the 26 cm × 25.6 cm × 254 µm UV-transmitting plastic window (Topas 8007x10, Topas Advanced Polymers, Florence, KY). Consistent with our previous experiments using this chamber²³,

the flow rate through the system was 12.5 L/min. The volume of the UV exposure region was 4.2 L so each aerosol was exposed for approximately 20 seconds as it traversed the window. The entire irradiation chamber was contained in a biosafety level 2 cabinet and all air inputs and outputs were equipped with HEPA filters (GE Healthcare Bio-Sciences, Pittsburgh, PA) to prevent unwanted contamination from entering or exiting the system.

Irradiation Chamber Performance. The custom irradiation chamber simulated the transmission of aerosolized viruses produced via human coughing and breathing. The chamber operated at an average relative humidity of 66% and an average temperature of 24° C across all runs. The average particle size distribution was 83% between 0.3 µm and 0.5 µm, 12% between 0.5 µm and 0.7 µm, and 5% > 0.7 µm (Table 3). Aerosolized viruses were efficiently transmitted through the system as evidenced from the control (zero exposure) showing clear virus integration (Figs. 2 and 3, top left panels).

Far-UVC Lamp and Dosimetry. The far-UVC source used in this study was a 12 W 222-nm KrCl excimer lamp module made by Ushio America (Item #9101711, Cypress, CA). The lamp is equipped with a proprietary optical filtering window to reduce lamp emissions outside of the 222 nm KrCl emission peak. The lamp was positioned 22 cm away from the exposure chamber window and directed at the center of the window. Optical power measurements were performed using an 818-UV/DB low-power UV enhanced silicon photodetector with an 843-R optical power meter (Newport, Irvine, CA).

Dosimetry was performed prior to starting an experiment to measure the irradiation fluence within the chamber at the position of the aerosol.

The distance between the lamp and the irradiation chamber permitted a single lamp to uniformly irradiate the entire exposure window area. Measurements using the silicon photodetector indicated an exposure intensity of approximately 90 µW/cm² across the exposure area. The chamber is equipped with a reflective aluminum surface opposite of the exposure window. As in our previous work with this chamber ²³, the reflectivity of this surface was approximately 15%. We have therefore conservatively estimated the intensity across the entire exposure area to be 100 µW/cm². With the lamp positioned

22 cm from the window and given the 20 seconds required for an aerosol particle to traverse the exposure window, we calculated the total exposure dose to a particle to be 2 mJ/cm². We used additional sheets of UV transmitting plastic windows to uniformly reduce the intensity across the exposure region to create different exposure conditions. While in our previous work with these sheets we measured a transmission closer to 65% ²³, for these tests we measured the 222-nm transmission of each sheet to be approximately 50%. This decrease in transmission is likely due to the photodegradation of the plastic over time ⁴. The addition of one or two sheets of the plastic covering the exposure window decreases the exposure dose to 1 and 0.5 mJ/cm², respectively.

Experimental Protocol. As previously described ²³, the virus solution in the nebulizer consisted of 1 ml of Modified Eagle's Medium (MEM, Life Technologies, Grand Island, NY) containing 10⁷-10⁸ TCID₅₀ of coronavirus, 20 ml of deionized water, and 0.05 ml of Hank's Balanced Salt Solution with calcium and magnesium (HBSS⁺⁺). The irradiation chamber was operated with aerosolized virus particles flowing through the chamber and the bypass channel for 5 minutes prior each sampling, in order to establish the desired RH value. Sample collection was initiated by changing air flow from the bypass channel to the BioSampler using the set of three way valves. The BioSampler was initially filled with 20 ml of HBSS⁺⁺ to capture the aerosol. During each sampling time, which lasted for 30 minutes, the inside of the irradiation chamber was exposed to 222-nm far-UVC light entering through the plastic window. Variation of the far-UVC dose delivered to aerosol particles was achieved by inserting additional UV-transparent plastic films as described above thereby delivering the three test doses of 0.5, 1.0 and 2.0 mJ/cm². Zero-dose control studies were conducted with the excimer lamp turned off. After the sampling period was completed the solution from the BioSampler was used for the virus infectivity assays.

Virus Infectivity Assays.

TCID₅₀. We used the 50% tissue culture infectious dose assay to determine virus infectivity ²⁸. Briefly, 10⁵ host cells were plated in each well of 96-well plates the day prior the experiment. Cells were

washed twice in HBSS⁺⁺ and serial 1:10 dilutions in infection medium of the exposed virus from the BioSampler was overlaid on cells for two hours. The cells were then washed twice in HBSS⁺⁺, covered with fresh infection medium, and incubated for three or four days at 34°C. Cytopathic effects (CPE) were scored at a bright field microscope (10x) as vacuolization of cytoplasm, cell rounding and sloughing. The TCID₅₀ was calculated with the Reed and Muench method^{28,35}. To confirm the CPE scores, the samples were fixed in 100% methanol for five minutes and stained with 0.1% crystal violet. The results are reported as the estimate of plaque forming units (PFU)/ml using the conversion PFU/ml = 0.7 TCID₅₀ by applying the Poisson distribution²⁹.

Immunofluorescence. To assess whether increasing doses of 222-nm light reduced the number of infected cells, we performed a standard fluorescent immunostaining protocol to detect a viral antigen in the host human cells²³. Briefly, 2x10⁵ host cells (MRC-5 cells for HCoV-229E and WI-38 for HCoV-OC43) were plated in each well of 48-well plates the day prior the experiment. After running through the irradiation chamber for 30 minutes, 150 µl of virus suspension collected from the BioSampler was overlaid on the monolayer of host cells. The cells were incubated with the virus for one hour, then washed three times with HBSS⁺⁺, and then incubated overnight in fresh infection medium. Infected cells were then fixed in 100% ice cold methanol at 4°C for 5 minutes and labeled with anti-human coronavirus spike glycoprotein (40021-MM07, Sino Biologicals, Chesterbrook, PA) 1:200 in HBSS⁺⁺ containing 1% bovine serum albumin (BSA; Sigma-Aldrich Corp. St. Louis, MO, USA) at room temperature for one hour with gentle shaking. Cells were washed three times in HBSS⁺⁺ and labeled with goat anti-mouse Alexa Fluor®-488 (Life Technologies, Grand Island, NY) 1:800 in HBSS⁺⁺ containing 1% BSA, at room temperature for 30 minutes in the dark with gentle shaking. Following three washes in HBSS⁺⁺, the cells were stained with Vectashield containing DAPI (4',6-diamidino-2-phenylindole) (Victor Laboratories, Burlingame, CA) and observed with the 10x objective of an Olympus IX70 fluorescent microscope equipped with a Photometrics PVCAM high-resolution, high-efficiency digital camera and Image-Pro Plus 6.0 software (Media Cybernetics, Bethesda, MD). For

each 222-nm dose and virus subgroup, the representative results were repeated twice. For each sample, up to ten fields of view of merged DAPI and Alexa Fluor®-488 images were acquired.

Data Analysis. The surviving fraction (S) of the virus was calculated by dividing the fraction PFU/ml at each UV dose (PFU_{UV}) by the fraction at zero dose ($\text{PFU}_{\text{controls}}$): $S = \text{PFU}_{\text{UV}}/\text{PFU}_{\text{controls}}$. Survival values were calculated for each repeat experiment and natural log (\ln) transformed to bring the error distribution closer to normal ³⁶. Robust linear regression using iterated re-weighted least squares (IWLS) ^{37,38} was performed in *R* 3.6.2 software using these normalized $\ln[S]$ values as the dependent variable and UV dose (D , mJ/cm^2) as the independent variable. Using this approach, the virus survival $[S]$ was described by first-order kinetics according to the equation ⁴:

$$\ln[S] = -k \times D[\text{Eq. 1}]$$

where k is the UV inactivation rate constant or susceptibility factor (cm^2/mJ). The regression was performed with the intercept term set to zero representing the definition of 100% relative survival at zero UV dose, separately for each studied virus strain. The data at zero dose, which by definition represent $\ln[S] = 0$, were not included in the regression. Uncertainties (95% confidence intervals, CI) for the k parameter for each virus strain were estimated by bootstrapping for each regression method because bootstrapping may result in more realistic uncertainty estimates, compared with the standard analytic approximation based on asymptotic normality, in small data sets such as those used here ($n = 3$ HCoV- 229E and $n = 4$ for HCoV-OC43). Goodness of fit was assessed by coefficient of determination (R^2). Analysis of residuals for autocorrelation and for heteroskedasticity was performed using the Durbin- Watson test ³⁹ and Breusch-Pagan test (implemented by *lmtest R* package) ⁴⁰, respectively. Parameter estimates (k) for each virus strain were compared with each other based on the 95% CIs and directly by t -test, using the sample sizes, k values, and their standard errors. The virus inactivation cross section, D_{90} , which is the UV dose that inactivates 90% of the exposed virus, was calculated as $D_{90} = -\ln[1 - 0.90]/k$. Other D values were calculated similarly.

References

1. World Health Organization. *Coronavirus disease (COVID-2019) situation reports*,

- 2020). https://www.who.int/emergencies/diseases/novel_coronavirus_2019/situation-reports
2. van Doremalen, N. *et al.* Aerosol and Surface Stability of SARS-CoV-2 as Compared with SARS-CoV-1. *New England Journal of Medicine*, doi:10.1056/NEJMc2004973 (2020).
 3. Bai, Y. *et al.* Presumed Asymptomatic Carrier Transmission of COVID-19. *JAMA*, doi:10.1001/jama.2020.2565 (2020).
 4. Kowalski, W. J. *Ultraviolet Germicidal Irradiation Handbook: UVGI for Air and Surface Disinfection*. (New York: Springer, 2009).
 5. Budowsky, E. I., Bresler, S. E., Friedman, E. A. & Zheleznova, N. V. Principles of selective inactivation of viral genome. I. UV-induced inactivation of influenza virus. *Arch Virol* **68**, 239- 247 (1981).
 6. Naunovic, Z., Lim, S. & Blatchley, E. R., 3rd. Investigation of microbial inactivation efficiency of a UV disinfection system employing an excimer lamp. *Water Res* **42**, 4838-4846, doi:10.1016/j.watres.2008.09.001 (2008).
 7. Trevisan, A. *et al.* Unusual high exposure to ultraviolet-C radiation. *Photochem Photobiol* **82**, 1077-1079 (2006).
 8. Zaffina, S. *et al.* Accidental exposure to UV radiation produced by germicidal lamp: case report and risk assessment. *Photochem Photobiol* **88**, 1001-1004, doi:10.1111/j.1751-1097.2012.01151.x (2012).
 9. Setlow, R. B., Grist, E., Thompson, K. & Woodhead, A. D. Wavelengths effective in induction of malignant melanoma. *Proc Natl Acad Sci U S A* **90**, 6666-6670 (1993).
 10. Balasubramanian, D. Ultraviolet radiation and cataract. *J Ocul Pharmacol Ther* **16**, 285-297, doi:10.1089/jop.2000.16.285 (2000).
 11. Narita, K. *et al.* 222-nm UVC inactivates a wide spectrum of microbial pathogens. *J*

- Hosp Infect*, doi:10.1016/j.jhin.2020.03.030 (2020).
12. Buonanno, M. *et al.* 207-nm UV Light - A Promising Tool for Safe Low-Cost Reduction of Surgical Site Infections. I: In Vitro Studies. *PLoS One* **8**, e76968, doi:10.1371/journal.pone.0076968 (2013).
 13. Buonanno, M. *et al.* 207-nm UV Light-A Promising Tool for Safe Low-Cost Reduction of Surgical Site Infections. II: In-Vivo Safety Studies. *PLoS One* **11**, e0138418, doi:10.1371/journal.pone.0138418 PONE-D-15-32644 [pii] (2016).
 14. Buonanno, *et al.* Germicidal Efficacy and Mammalian Skin Safety of 222-nm UV Light. *Radiation Research* **187**, 483-491, doi:10.1667/RR0010CC.1 (2017).
 15. Ponnaiya, B. *et al.* Far-UVC light prevents MRSA infection of superficial wounds in vivo. *PLOS ONE* **13**, e0192053, doi:10.1371/journal.pone.0192053 (2018).
 16. Narita, K. *et al.* Disinfection and healing effects of 222-nm UVC light on methicillin-resistant *Staphylococcus aureus* infection in mouse wounds. *Journal of Photochemistry and Photobiology B: Biology* **178**, 10-18, doi:<https://doi.org/10.1016/j.jphotobiol.2017.10.030> (2018).
 17. Narita, K., Asano, K., Morimoto, Y., Igarashi, T. & Nakane, A. Chronic irradiation with 222-nm UVC light induces neither DNA damage nor epidermal lesions in mouse skin, even at high doses. *PLoS One* **13**, e0201259, doi:10.1371/journal.pone.0201259 (2018).
 18. Yamano, N. *et al.* Long-term effects of 222 nm ultraviolet radiation C sterilizing lamps on mice susceptible to ultraviolet radiation. *Photochem Photobiol*, doi:10.1111/php.13269 (2020).
 19. Goldfarb, A. R. & Saidel, L. J. Ultraviolet absorption spectra of proteins. *Science* **114**, 156-157 (1951).
 20. Setlow, J. in *Current topics in radiation research II* (eds Ebert M & Howard A) 195-248

(North Holland Publishing Company, 1966).

21. Coohill, T. P. Virus-cell interactions as probes for vacuum-ultraviolet radiation damage and *Photochemistry and photobiology* **44**, 359-363 (1986).
22. Green, H., Boll, J., Parrish, J. A., Kochevar, I. E. & Oseroff, A. R. Cytotoxicity and mutagenicity of low intensity, 248 and 193 nm excimer laser radiation in mammalian cells. *Cancer research* **47**, 410-413 (1987).
23. Welch, D. *et al.* Far-UVC light: A new tool to control the spread of airborne-mediated microbial diseases. *Scientific Reports* **8**, 2752, doi:10.1038/s41598-018-21058-w (2018).
24. Fehr, R. & Perlman, S. Coronaviruses: an overview of their replication and pathogenesis. *Methods Mol Biol* **1282**, 1-23, doi:10.1007/978-1-4939-2438-7_1 (2015).
25. Woo, P. C., Huang, Y., Lau, S. K. & Yuen, K. Y. Coronavirus genomics and bioinformatics analysis. *Viruses* **2**, 1804-1820, doi:10.3390/v2081803 (2010).
26. Papineni, R. S. & Rosenthal, F. S. The Size Distribution of Droplets in the Exhaled Breath of Healthy Human Subjects. *Journal of Aerosol Medicine* **10**, 105-116, doi:10.1089/jam.1997.10.105 (1997).
27. Sparrow, A. H., Underbrink, A. G. & Sparrow, R. C. Chromosomes and cellular radiosensitivity. I. The relationship of D₀ to chromosome volume and complexity in seventy-nine different organisms. *Radiat Res* **32**, 915-945 (1967).
28. Lindenbach, B. D. Measuring HCV infectivity produced in cell culture and in vivo. *Methods Mol Biol* **510**, 329-336, doi:10.1007/978-1-59745-394-3_24 (2009)
29. Mahy, B. K., H. . *Virology Methods manual*. (Academic Press, 1996).
30. Bjorck, A. *Numerical Methods For Linear Least Squares Problems*. (1996).
31. Walls, A. C. *et al.* Tectonic conformational changes of a coronavirus spike

- glycoprotein promote membrane fusion. *Proc Natl Acad Sci U S A* **114**, 11157-11162, doi:10.1073/pnas.1708727114 (2017).
32. Madu, I. G., Roth, S. L., Belouzard, S. & Whittaker, G. R. Characterization of a highly conserved domain within the severe acute respiratory syndrome coronavirus spike protein S2 domain with characteristics of a viral fusion peptide. *J Virol* **83**, 7411-7421, doi:10.1128/JVI.00079-09 (2009).
33. Walker, M. & Ko, G. Effect of Ultraviolet Germicidal Irradiation on Viral Aerosols. *Environmental Science & Technology* **41**, 5460-5465, doi:10.1021/es070056u (2007).
34. The International Commission on Non-Ionizing Radiation Protection. Guidelines on limits of exposure to ultraviolet radiation of wavelengths between 180 nm and 400 nm (Incoherent optical radiation). *Health Physics* **87**, 171-186 (2004).
35. Reed, L. J. a. M., H. A simple method of estimating fifty per cent endpoints. *American Journal of Epidemiology* **Volume 27**, 493-497 (1938).
36. Keene, O. N. The log transformation is special. *Stat Med* **14**, 811-819 (1995).
37. Venables, W. N., Ripley, B. D. & Venables, W. N. *Modern applied statistics with S*. 4th edn, (Springer, 2002).
38. Marazzi, *Algorithm, Routines, and S functions for Robust Statistics*. (Wadsworth & Brooks/cole, 1993).
39. Durbin, & Watson, G. S. Testing for serial correlation in least squares regression. I. *Biometrika* **37**, 409-428 (1950).
40. Breusch, T., & Pagan, A. A Simple Test for Heteroscedasticity and Random Coefficient *Econometrica* **47**, 1287-1294., doi:10.2307/1911963 (1979).

Declarations

Acknowledgements

This work was supported by the Shostack Foundation and by NIH grant R42-AI125006-03. We thank

Dr. Alan W. Bigelow and Gary W. Johnson for initial design and construction of the aerosol chamber, and Dr. Gerhard Randers-Pehrson for his conceptual insights.

Author Contributions

M.B. performed the biological experiments and analyzed the data; D.W. performed the chamber setup and lamp dosimetry; I. S. performed the statistical analysis; D.J.B. supervised the studies and contributed conceptual advice. All authors contributed in preparation of the manuscript. The authors declare no competing interests.

Tables

Table 1: Linear regression parameters for normalized $\ln[S]$ [survival] values (Eq. 1) as the dependent variable and UV dose (D , mJ/cm^2) as the independent variable. k is the UV inactivation rate constant or susceptibility factor (cm^2/mJ). The linear regression was performed with the intercept term set to zero representing the definition of 100% relative survival at zero UV dose. The coronavirus inactivation cross section, D_{90} (the UV dose that inactivates 90% of the exposed virus) was calculated using $D_{90} = -\ln[1 - 0.90]/k$.

Human coronavirus type	k (cm^2/mJ)	k 95% confidence interval		p value	R2	D90 (mJ/cm^2)
		<i>Lower</i>	<i>Upper</i>			
HCoV-229E	4.1	2.5	4.8	0.0003	0.86	0.56
HCoV-OC43	5.9	3.8	7.1	0.0001	0.78	0.39

Table 2: Estimated k , D_{99} , and $D_{99.9}$ values for exposure to 222 nm far-UVC light

for alphacoronavirus

HCoV-229E, betacoronavirus HCoV-OC43, and influenza A (H1N1).

Species	k (cm ² /mj)	D_{90} (mj/cm ²)	D_{99} (mj/cm ²)	
HCoV-229E	4.1	0.56	1.1	
HCoV-OC43	5.9	0.39	0.78	
Influenza A (H1N1)*	1.8	1.3	2.6	

* D_{99} , and $D_{99,9}$ values for influenza A (H1N1) denote extrapolated values, as these doses were not used during testing ²³.

Our previous work with H1N1 utilized the fluorescent focus assay ²³, while the current work with coronaviruses used the TCID₅₀ assay.

Table 3. Example of particle size distributions from humans during various activities are given ²⁶ along with the averaged measured values for this work.

		Particle Size Distribution	
		< 1.0 μm	> 1.0 μm
Papineni et al. ²⁶	Coughing	83%-91%	9%-17%
	Mouth Breathing	83%-95%	4%-17%
	Nose Breathing	83%-100%	0-17%
	Talking	77%-88%	11%-23%
This work		0.3-0.5 μm	0.5-0.7 μm
		83%	12%

Figures

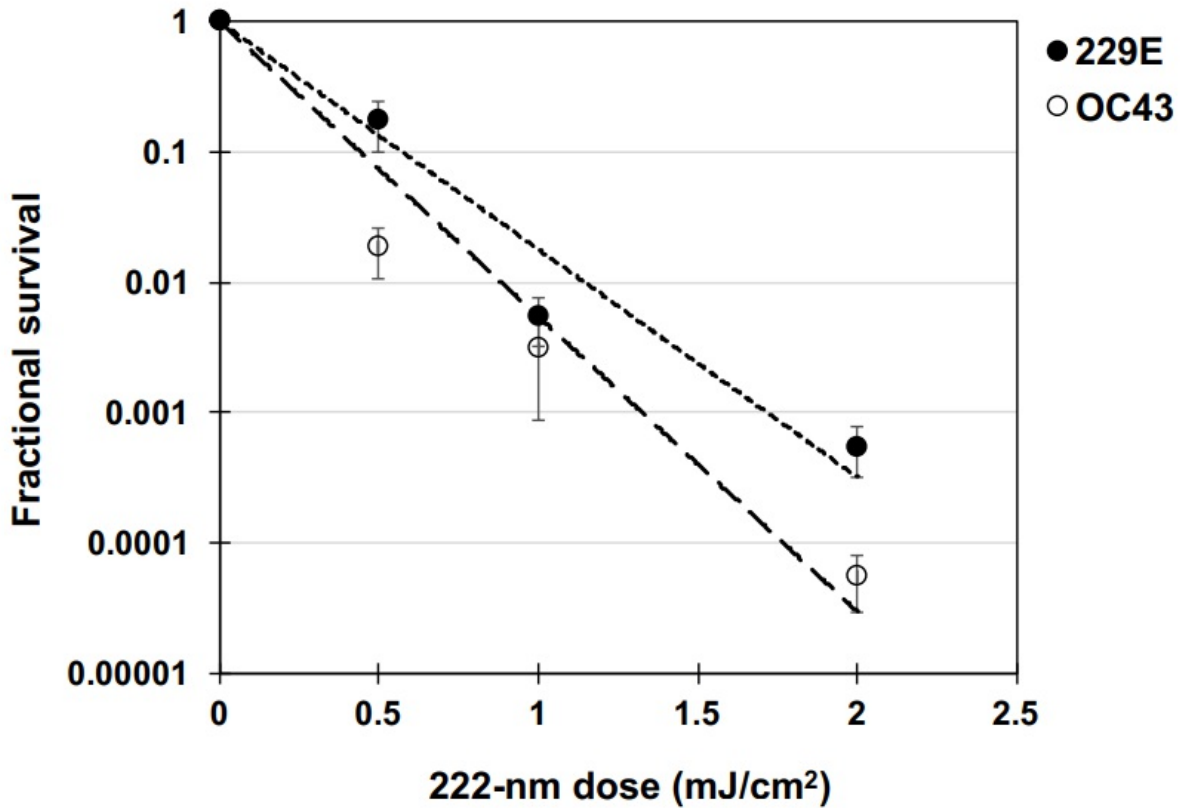


Figure 1

Coronavirus survival as function of the dose of far-UVC light. Fractional survival, PFUUV / PFUcontrols, is plotted as a function of the 222-nm far-UVC dose. The results are reported as the estimate plaque forming units (PFU)/ml using the conversion PFU/ml = 0.7 TCID₅₀ 29 by applying the Poisson distribution. Values are reported as mean ± SEM from multiple experiments (n=3 alpha HCoV-229E and n=4 for beta HCoV-OC43); the lines represent the best-fit regressions to Eq. 1 (see text and Table 1).

Alpha HCoV-229E in normal human lung MRC5 fibroblasts
Green = Anti-human coronavirus spike glycoprotein; Blue= DAPI

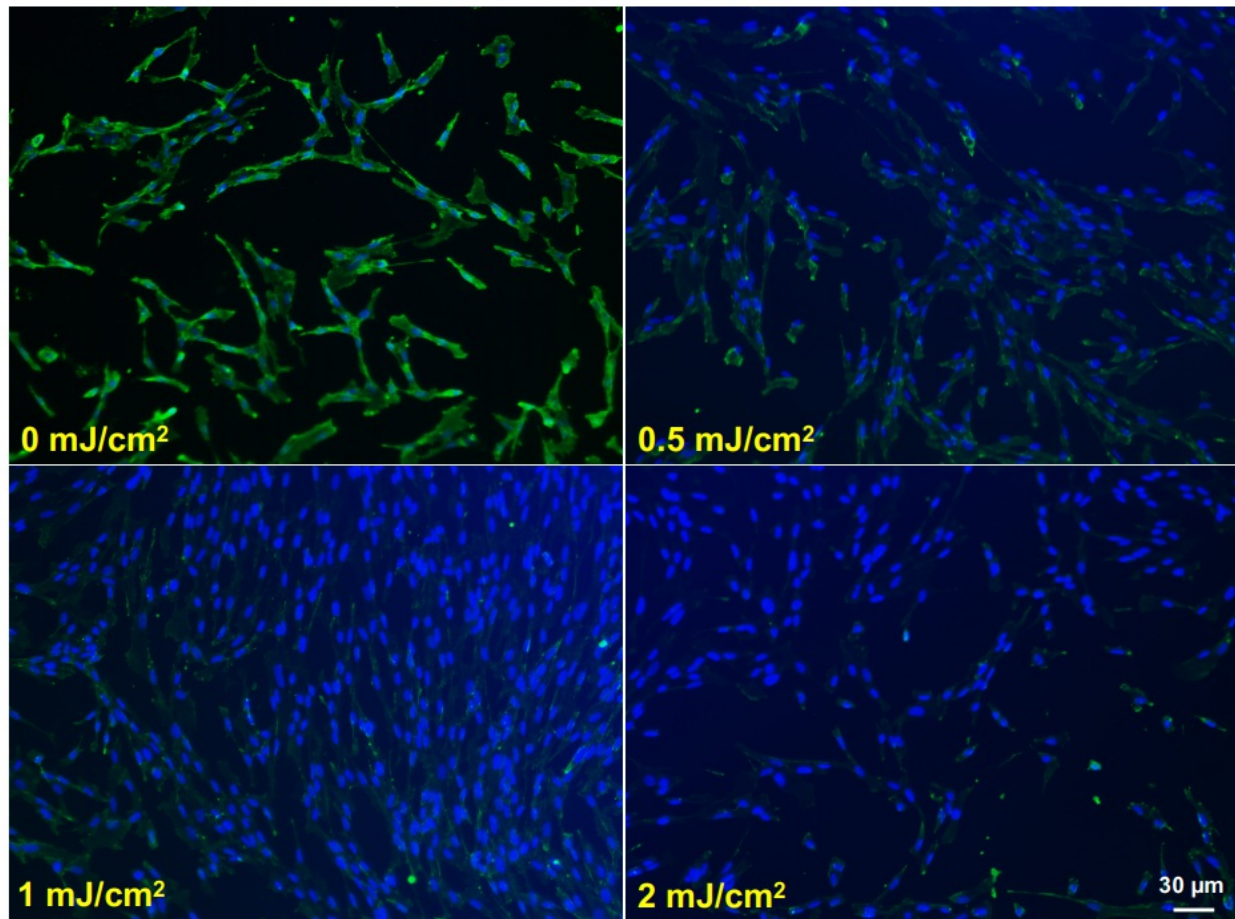


Figure 2

Infection of human lung cells from irradiated aerosolized alpha HCoV-229E as function of dose of far-UVC light. Representative fluorescent images of MRC-5 normal human lung fibroblasts infected with human alphacoronavirus 229E exposed in aerosolized form. The viral solution was collected from the BioSampler after running through the aerosol chamber while being exposed to 0, 0.5, 1 or 2 mJ/cm² of 222-nm light. Green fluorescence qualitatively indicates infected cells (Green= Alexa Fluor®-488 used as secondary antibody against anti- human coronavirus spike glycoprotein antibody; Blue = nuclear stain DAPI). Images were acquired with a 10x objective; the scale bar applies to all the panels in the figure.

Beta HCoV-OC43 in normal human lung WI-38 fibroblasts
Green = Anti-human coronavirus spike glycoprotein; Blue= DAPI

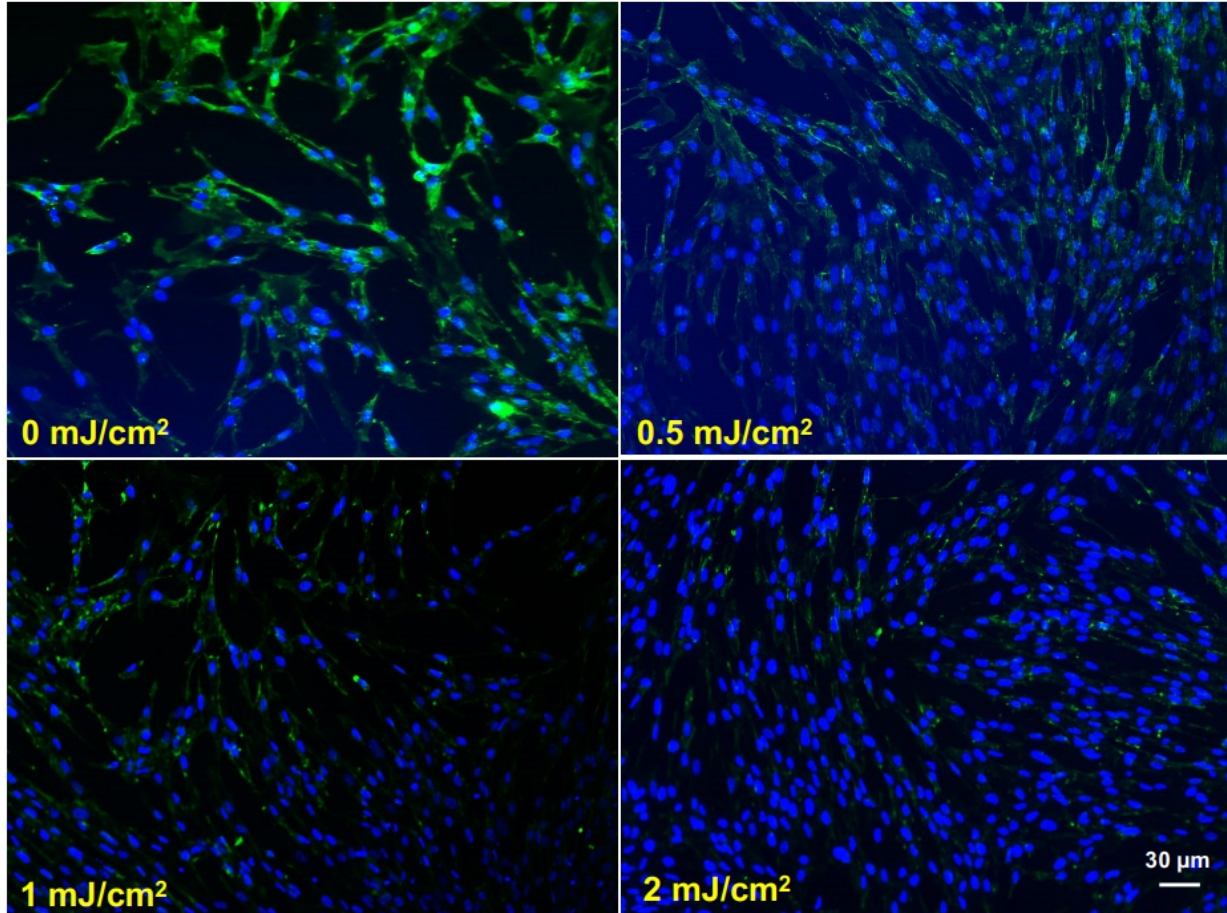


Figure 3

Infection of human lung cells from irradiated aerosolized beta HCoV-OC43 as function of dose of far-UVC light. Representative fluorescent images of WI-38 normal human lung fibroblasts infected with human betacoronavirus OC43 exposed in aerosolized form. The viral solution was collected from the BioSampler after running through the aerosol chamber while being exposed to 0, 0.5, 1 or 2 mJ/cm² of 222-nm light. Green fluorescence qualitatively indicates infected cells (Green= Alexa Fluor®-488 used as secondary antibody against anti-human coronavirus spike glycoprotein antibody; Blue = nuclear stain DAPI,). Images were acquired with a 10x objective; the scale bar applies to all the panels in the figure.